Electronic Supplementary Information (ESI)

# 3D Yolk-Shelled $NiGa_2S_4$ Microspheres Confined with Nanosheets for High Performance Supercapacitors

Shude Liu,[a] Kwang Ho Kim,[b,c*] Je Moon Yun,[c] Aniruddha Kundu,[a] K. Vijaya Sankar,[a] Umakant M Patil,[a] Chaiti Ray,[a] Seong Chan Jun,[a*]

[a]Nano-Electro Mechanical Device Laboratory, School of Mechanical Engineering, Yonsei University, Seoul 120-749, South Korea
[b]Department of Materials Science and Engineering, Pusan National University, San 30 Jangjeon-dong, Geumjeong-gu, Busan 609-735, South Korea
[c]Global Frontier R&D Center for Hybrid Interface Materials, Pusan National University, 30 Jangjeon-dong, Geumjung-gu, Busan 609-735, South Korea

*E-mail: scj@yonsei.ac.kr *(Seong Chan Jun)*
kwhokim@pusan.ac.kr (*Kwang Ho Kim*)

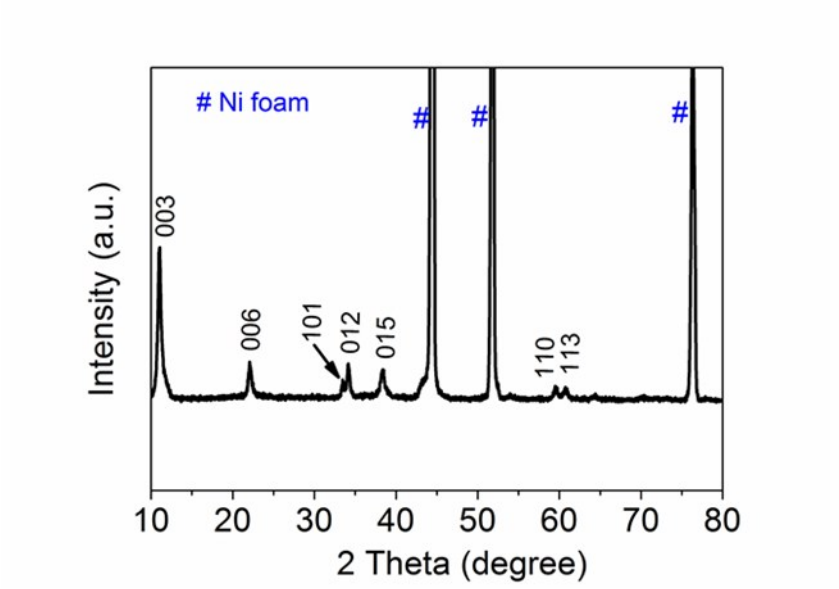


Figure S1 XRD pattern of the as-synthesized NiGa-LDH.

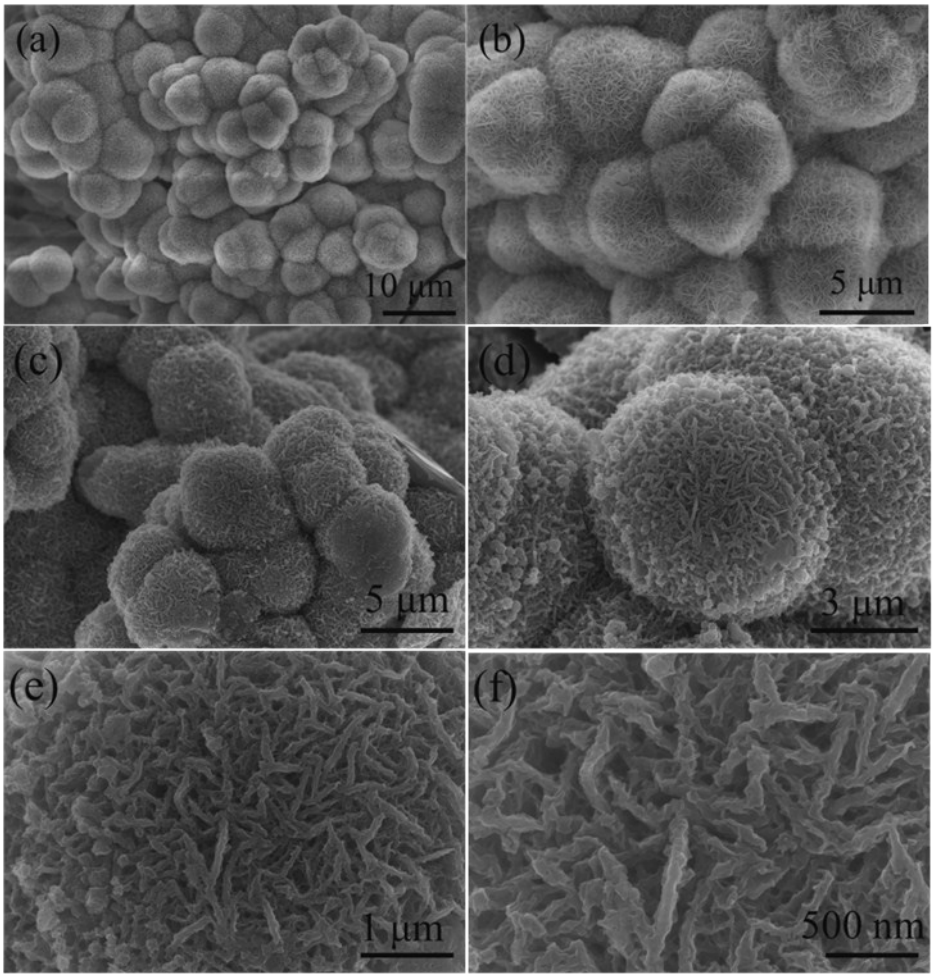


Figure S2 SEM images of the NiGa-LDH (a, b) and $NiGa_2S_4$-N2 (c-f) at different magnifications.

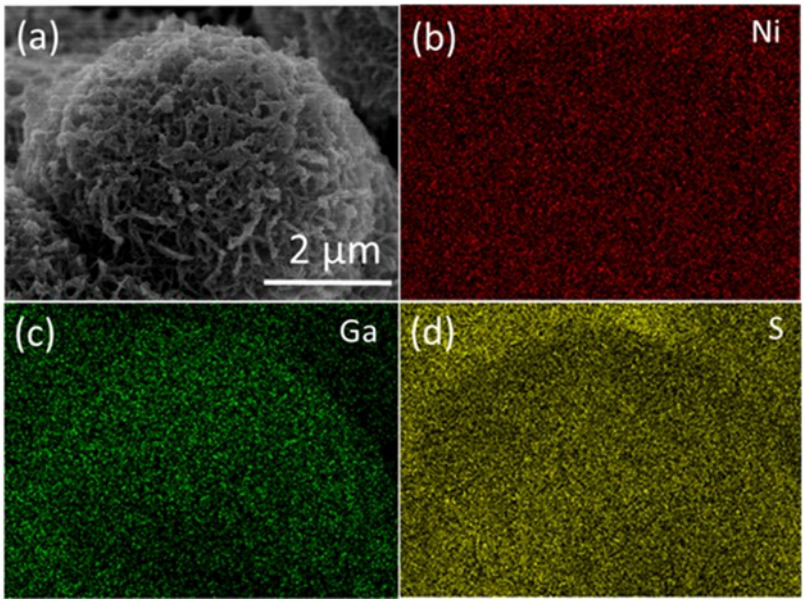


Figure S3 (a) SEM image of the $NiGa_2S_4$-N2, and elemental mapping of (b) Ni, (c) Ga and (d) S, respectively.

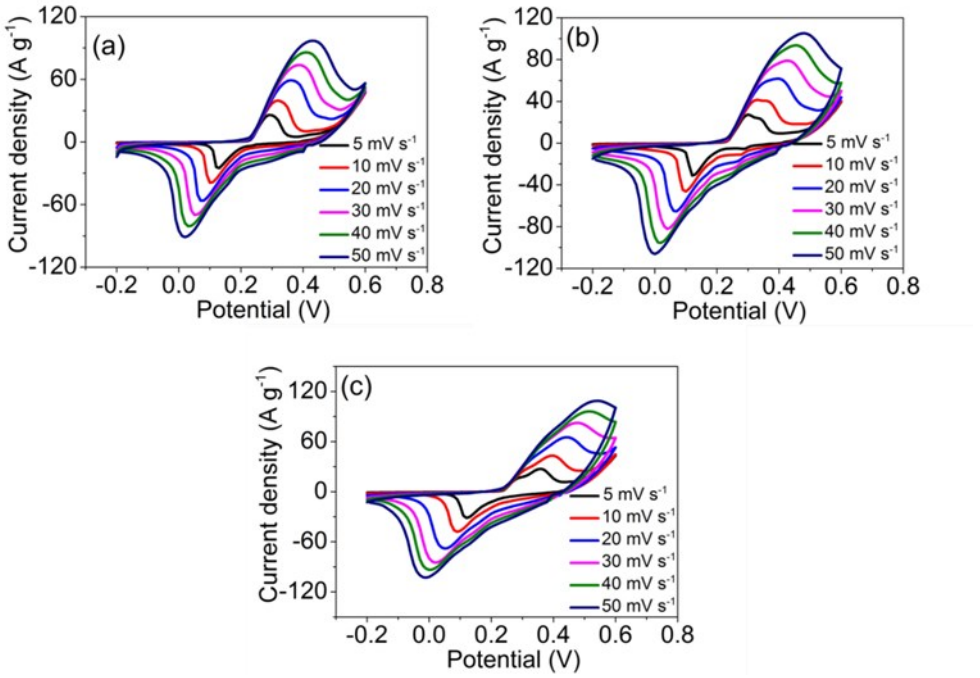


Figure S4 CV curves of (a) NiGa-LDH, (b) $NiGa_2S_4$-N1, and (c) $NiGa_2S_4$-N3 electrodes recorded at different scan rates.

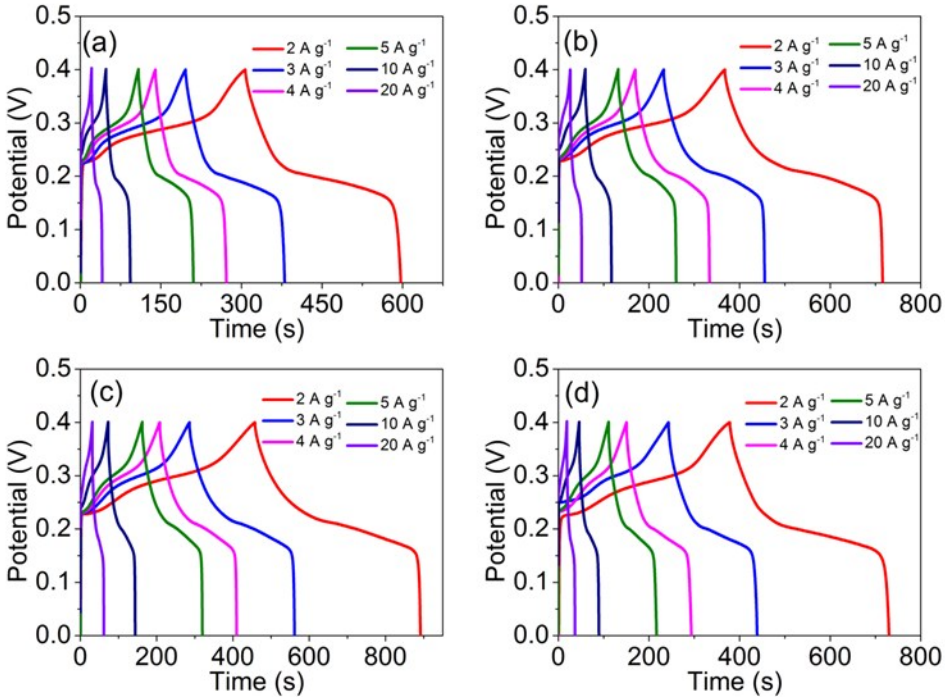


Figure S5 GCD curves of (a) NiGa-LDH, (b) $NiGa_2S_4$-N1, (c) $NiGa_2S_4$-N2, and (c) $NiGa_2S_4$-N3 electrodes measured at different current densities.

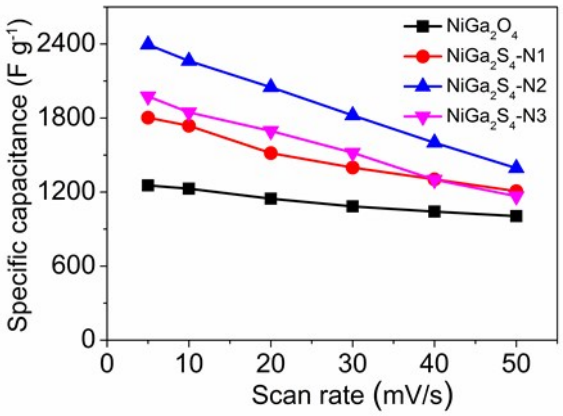


Figure S6 Specific capacitances of NiGa-LDH, $NiGa_2S_4$-N1, $NiGa_2S_4$-N2, and $NiGa_2S_4$-N3 electrodes measured at different scan rates.

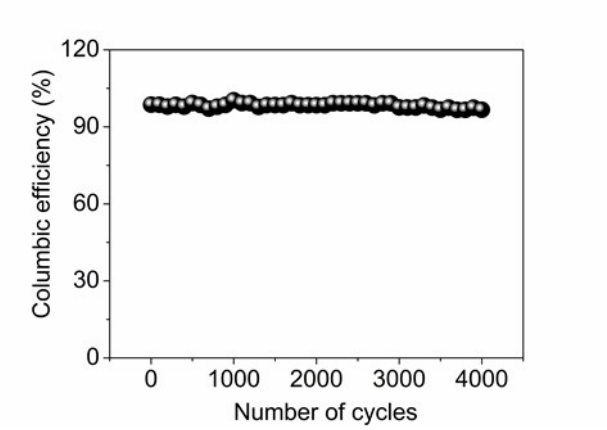


Figure S7 Columbic efficiency of $NiGa_2S_4$-N2 electrode during cycling test.

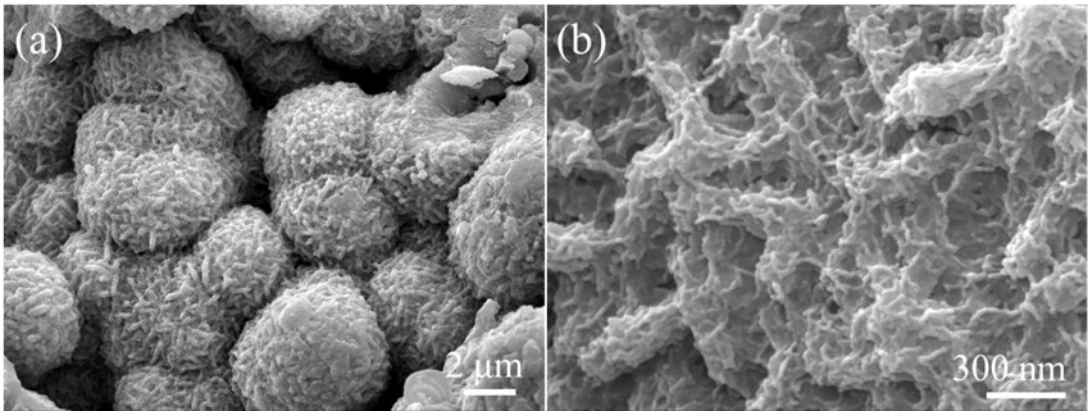


Figure S8 SEM images of $NiGa_2S_4$-N2 electrode after cycling test.

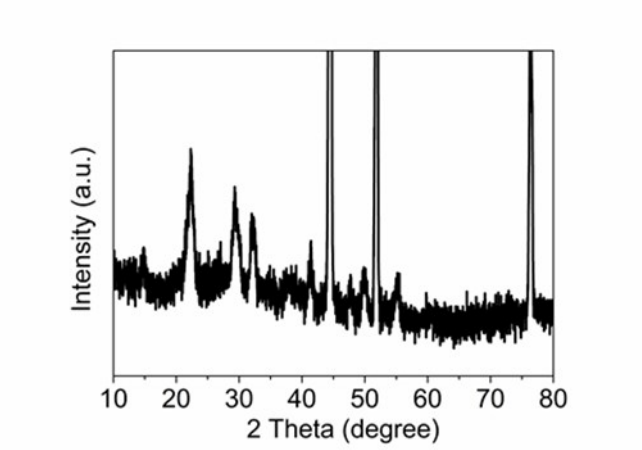


Figure S9 XRD pattern of $NiGa_2S_4$-N2 electrode after cycling test.

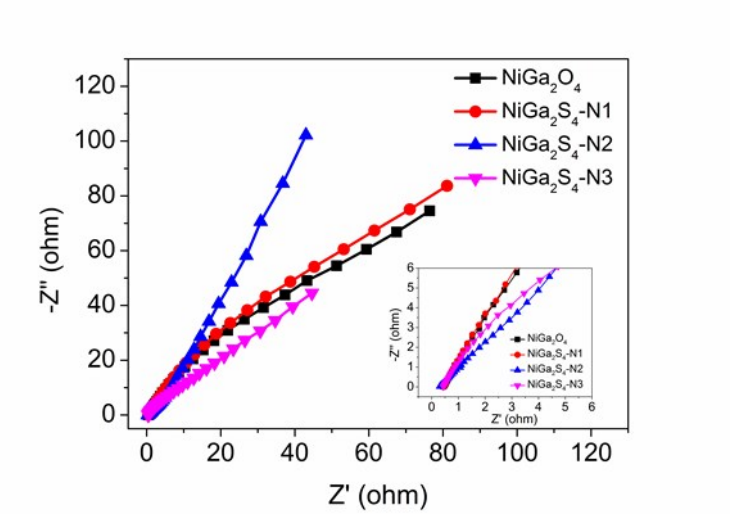


Figure S10 Comparison of Nyquist plots of electrodes of NiGa-LDH, $NiGa_2S_4$-N1, $NiGa_2S_4$-N2, and $NiGa_2S_4$-N3 electrodes. The inset shows the enlarged EIS in the high frequency region.

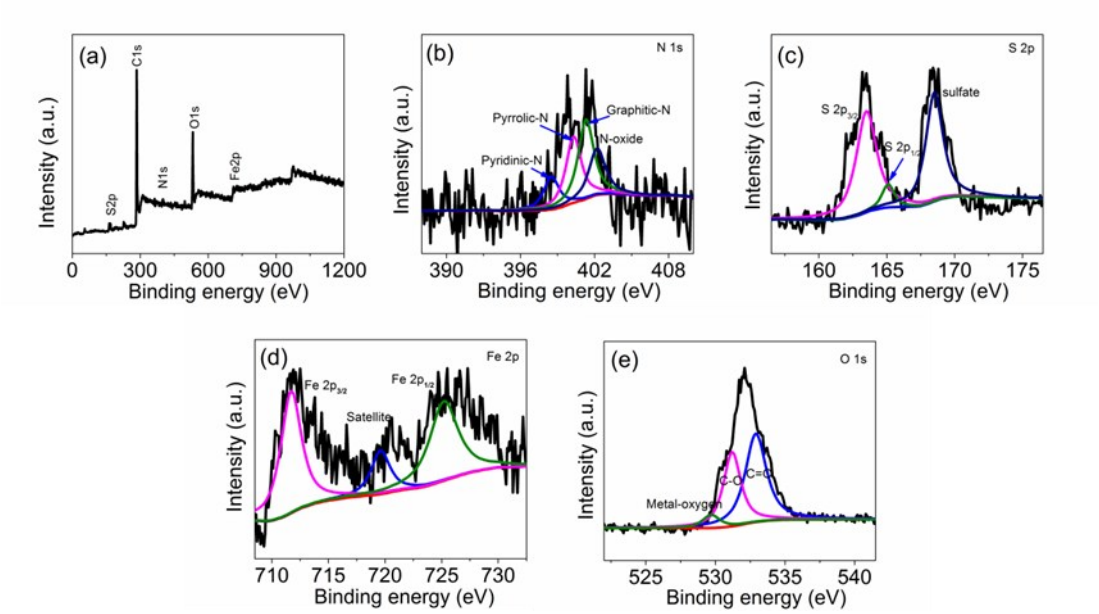


Figure S11 (a) XPS spectra of the as-prepared N,S-G/$Fe_2O_3$. XPS survey scan of (b) N 2p, (c) S 2p, (d) Fe 2p, and (e) O 1s for N,S-G/$Fe_2O_3$.

The high-resolution N 1s spectrum of N,S-G can be deconvoluted into four peaks at binding energies of around 398.5, 400.3, 401.3, and 402.2 eV (Figure S11b), corresponding to pyridinic N, pyrrolic N, graphitic N, and N oxides of pyridinic N, respectively.[1, 2] The complex S 2p spectrum can be resolved into three separate peaks (Figure S11c). The first two peaks can be assigned to $2p_{3/2}$ and $2p_{1/2}$ positions at binding energies of around 163.5 and 165.1 eV, respectively. Moreover, the peak at 168.5 eV is attributed to sulfate species formed by oxidation of sulfur in air.[3, 4] The Fe 2p spectrum (Figure S11d) presents two peaks with binding energies of 711.7 and 725.2 eV, which correspond to the Fe $2p_{3/2}$ and Fe $2p_{1/2}$ spin–orbit interaction of $Fe_2O_3$, respectively, indicating the existence of $Fe^{3+}$. Additionally, the satellite peak of the Fe $2p_{3/2}$ line centered at 719.3 eV is detected, further revealing the presence of $Fe^{3+}$ species.[5, 6] The O 1s spectrum (Figure S11e) is deconvolved into three bands at 529.7, 531.2, and 532.9 eV, corresponding to metal–oxygen bonds, C–O bonds, and C=O bond structures, respectively.

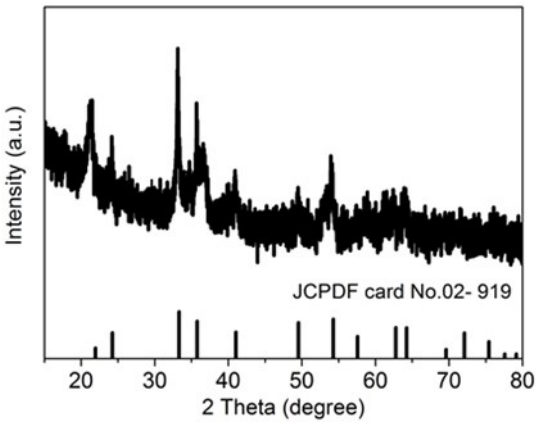


Figure S12 XRD pattern of the as-prepared N,S-G/$Fe_2O_3$ particles.

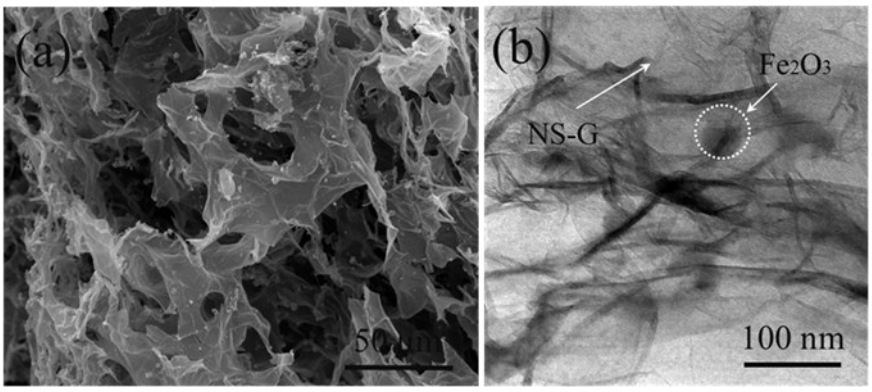


Figure S13 (a) SEM image and (b) TEM image of N,S-G/$Fe_2O_3$.

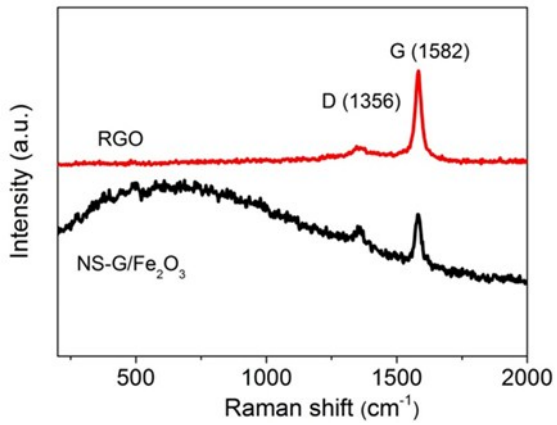


Figure S14 Raman spectra of the as-prepared RGO and N,S-G/$Fe_2O_3$.

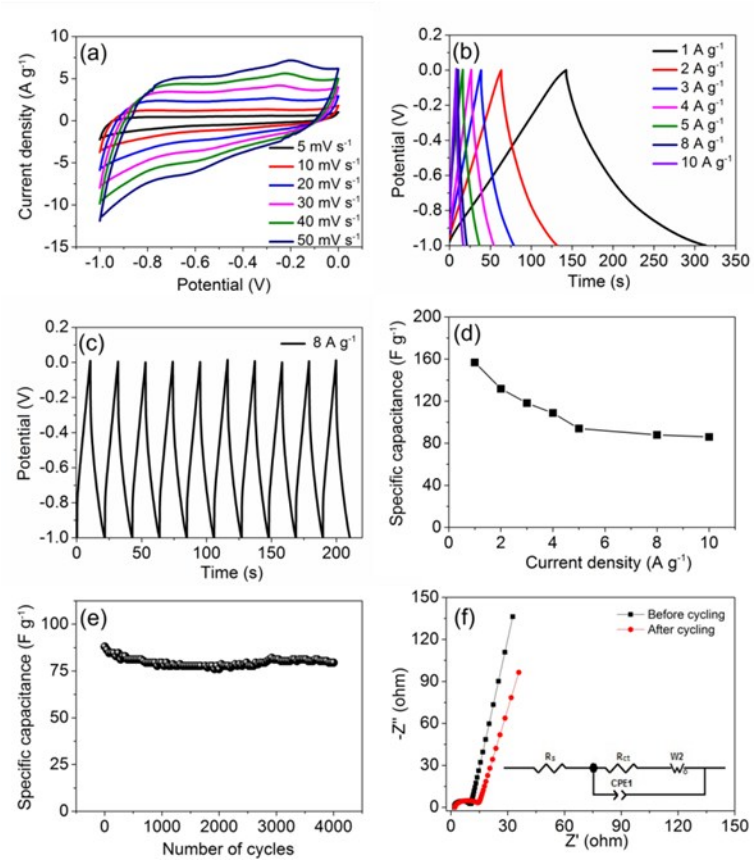


Figure S15 Electrochemical performance of N,S-G/$Fe_2O_3$: (a) CV curves collected in 6 M KOH as a function of scan rate, (b) GCD profiles obtained at different current densities, (c) the first eight cycles at a current density of 8 A $g^{-1}$, (d) specific capacitance calculated as a function of current density, (e) cycling stability tested at 5 A $g^{-1}$ for 4000 cycles, (f) Nyquist plots obtained in a frequency range of $10^{-2}$ to $10^5$ Hz at the open-circuit potential before and after the cycling test (inset: fitted equivalent circuit).

All of the N,S-G/$Fe_2O_3$ CV curves show a quasi-rectangular shape (Figure S15a), indicating that the capacitance originates mainly from double-layer capacitance and pseudocapacitive behavior at the electrode interface.[7, 8] Figure S15b exhibits a typical symmetrical triangular curve, indicating the excellent reversibility of the as-prepared N,S-G/$Fe_2O_3$.[8] The GCD curve of the first eight cycles (Figure S15c) clearly indicates good electrochemical reversibility with around 99% Columbic efficiency. The specific capacitances of the N,S-G/$Fe_2O_3$ electrode (Figure S15d) calculated from the GCD profiles are 157, 132, 118, 109, 94, 88, and 86 F $g^{-1}$ at current densities of 1, 2, 3, 4, 5, 8, and 10 A $g^{-1}$, respectively. After 4000 cycles, the about 90.3% of the initial capacitance is retained even at a current density of 5 A $g^{-1}$ (Figure S15e). The Nyquist plots of the N,S-G/$Fe_2O_3$ electrode show no obvious change after the cycling test (Figure S15f), implying noteworthy stability of the electrode.

**Table S1 Electrochemical performances comparison of the yolk-shelled $NiGa_2S_4$ structure with previously reported transition metal sulfides.**

| **Materials** | Specific capacitance | Current destiny/scan rate | Ref. |
|---|---|---|---|
| **$Co_9S_8$ nanorod** | 783.3 F $g^{-1}$ | 5 mV $s^{-1}$ | S9 |
| **$Co_9S_8$ nanofilm** | 1645 F $g^{-1}$ | 3 A $g^{-1}$ | S10 |
| **$Co_9S_8$ nanotube** | 390 F $g^{-1}$ | 5 mV $s^{-1}$ | S11 |
| **$CoS_2$ nanoparticle/graphene** | 253 F $g^{-1}$ | 5 mV $s^{-1}$ | S12 |
| **$Ni_2S$ hollow sphere** | 547.2 F $g^{-1}$ | 0.6 A $g^{-1}$ | S13 |
| **NiS hollow microsphere** | 1636.4 F $g^{-1}$ | 1 A $g^{-1}$ | S14 |
| **NiS/CoO nanosheet hybrid** | 1054 F $g^{-1}$ | 6 A $g^{-1}$ | S15 |
| **$NiCo_2S_4$ hollow sphere** | 1753.2 F $g^{-1}$ | 1 A $g^{-1}$ | S16 |
| **$NiCo_2S_4$ nanosheet** | 744 F $g^{-1}$ | 1 A $g^{-1}$ | S17 |
| **$NiCo_2S_4$ nanotube** | 1093 F $g^{-1}$ | 0.2 A $g^{-1}$ | S18 |
| **$NiCo_2S_4$ nanotube@$MnO_2$ nanoplate** | 1337.8 F $g^{-1}$ | 2 A $g^{-1}$ | S19 |
| **$Ni_3S_2$@CoS core–shell nano-triangular pyramid arrays** | 376.06 F $g^{-1}$ | 4 mA $cm^{-2}$ | S20 |
| **$NiCo_2S_4$@$Co(OH)_2$ core-shell nanotube arrays** | 1054.95 F $g^{-1}$ | 2 mA $cm^{-2}$ | S21 |
| **α-MnS nanoparticle/N doping-rGO** | 933.6 F $g^{-1}$ | 1 A $g^{-1}$ | S22 |
| **γ-MnS particle/rGO** | 846.4 F $g^{-1}$ | 5 mV $s^{-1}$ | S23 |
| **yolk-shelled $NiGa_2S_4$** | 1798 F $g^{-1}$ | 2 A $g^{-1}$ | Present work |

**Table S2 Comparison of electrochemical performance of the reported asymmetric supercapacitor devices and the assembled $NiGa_2S_4$//N,S-G/$Fe_2O_3$.**

| **Asymmetric supercapacitor devices** | Energy density (Wh $kg^{-1}$) | Power density (W $kg^{-1}$) | Current density (A $g^{-1}$ or mA $cm^{-2}$) | Specific capacitance (A $g^{-1}$) | Mass ratio of positive/negative | Ref. |
|---|---|---|---|---|---|---|
| **$CoNi_2S_4$//AC** | 33.9 (27.2) | 409 (2458) | 10 (60) mA $cm^{-2}$ | / | / | S24 |
| **NiS–rGO//AC** | 18.7 (11.6) | 124 (2900) | 0.2 (4) A $g^{-1}$ | 79.7 (49.5) | / | S25 |
| **$Ni_3S_2$/MWCNTs//AC** | 31.4 (26.3) | 200 (4000) | 1 (16) A $g^{-1}$ | 55.8 (35) | 0.21 | S26 |
| **$Co_9S_8$//AC** | 31.4 | 200 | 0.25 A $g^{-1}$ | 82.9 | / | S27 |
| **$NiCo_2S_4$@$Ni_3V_2O_8$// AC** | 42.7 | 200 | 0.5 A $g^{-1}$ | 93.75 | 0.51 | S28 |
| **$NiCo_2S_4$@$Co(OH)_2$// AC** | 35.89 | 400 | 0.5 A $g^{-1}$ | 100.94 | 0.40 | S29 |
| **$(Ni Co)_{0.85}Se$//graphene** | ~ 24.3 | ~1094 | 8 mA $cm^{-2}$ | ~ 54 | / | S30 |
| **$NiGa_2S_4$//N,S-G/$Fe_2O_3$** | 43.6 (22.2) | 961 (15,974) | 1.5 (24) A $g^{-1}$ | 123(63) | 0.14 | Present work |

S1. E. Bi, H. Chen, X. Yang, F. Ye, M. Yin and L. Han, *Scientific reports*, 2015, **5**, 13214
S2. B. Kumar, M. Asadi, D. Pisasale, S. Sinha-Ray, B. A. Rosen, R. Haasch, J. Abiade, A. L. Yarin and A. Salehi-Khojin, *Nature communications*, 2013, **4**, 2819.
S3. B. Quan, S.-H. Yu, D. Y. Chung, A. Jin, J. H. Park, Y.-E. Sung and Y. Piao, *Scientific reports*, 2014, **4**, 5639
S4. G. Li, J. Sun, W. Hou, S. Jiang, Y. Huang and J. Geng, *Nature communications*, 2016, 7, 10601.
S5. Y. Zeng, Y. Han, Y. Zhao, Y. Zeng, M. Yu, Y. Liu, H. Tang, Y. Tong and X. Lu, *Advanced Energy Materials*, 2015, **5**, 1402176.
S6. C. Pereira, A. M. Pereira, P. Quaresma, P. B. Tavares, E. Pereira, J. P. Araújo and C. Freire, *Dalton Transactions*, 2010, **39**, 2842-2854.
S7. P. Yang, Y. Ding, Z. Lin, Z. Chen, Y. Li, P. Qiang, M. Ebrahimi, W. Mai, C. P. Wong and Z. L. Wang, *Nano letters*, 2014, **14**, 731-736.
S8. S. Gu, Z. Lou, L. Li, Z. Chen, X. Ma and G. Shen, *Nano Research*, 2016, **9**, 424-434.
S9. J. Xu, Q. Wang, X. Wang, Q. Xiang, B. Liang, D. Chen and G. Shen, *ACS nano*, 2013, 7, 5453-5462.
S10. H. Li, Y. Gao, Y. Shao, Y. Su and X. Wang, *Nano letters*, 2015, **15**, 6689-6695.
S11. J. Yu, H. Wan, J. Jiang, Y. Ruan, L. Miao, L. Zhang, D. Xia and K. Xu, *Journal of The Electrochemical Society*, 2014, **161**, A996-A1000.
S12. B. Wang, J. Park, D. Su, C. Wang, H. Ahn and G. Wang, *Journal of Materials Chemistry*, 2012, **22**, 15750-15756.
S13. C. Wei, C. Cheng, Y. Cheng, Y. Wang, Y. Xu, W. Du and H. Pang, *Dalton Transactions*, 2015, **44**, 17278-17285.
S14. Z. Li, A. Gu, J. Sun and Q. Zhou, *New Journal of Chemistry*, 2016, **40**, 1663-1670.
S15. J. Wu, C. Ouyang, S. Dou and S. Wang, *Nanotechnology*, 2015, **26**, 325401.
S16. Z. Li, Y. Qu, M. Wang, Y. Hu, J. Han, L. Fan and R. Guo, *Colloid and Polymer Science*, 2016, 1-8.
S17. Z. Wu, X. Pu, X. Ji, Y. Zhu, M. Jing, Q. Chen and F. Jiao, *Electrochimica Acta*, 2015, **174**, 238-245.
S18. H. Wan, J. Jiang, J. Yu, K. Xu, L. Miao, L. Zhang, H. Chen and Y. Ruan, *CrystEngComm*, 2013, **15**, 7649-7651.
S19. J. Yang, M. Ma, C. Sun, Y. Zhang, W. Huang and X. Dong, *Journal of Materials Chemistry A*, 2015, **3**, 1258-1264.
S20. R. Li, S. Wang, J. Wang and Z. Huang, *Physical Chemistry Chemical Physics*, 2015, **17**, 16434-16442.
S21. R. Li, S. Wang, Z. Huang, F. Lu and T. He, *Journal of Power Sources*, 2016, **312**, 156-164.
S22. H. Quan, B. Cheng, D. Chen, X. Su, Y. Xiao and S. Lei, *Electrochimica Acta*, 2016, **210**, 557 - 566.
S23. X. Li, J. Shen, N. Li and M. Ye, *Journal of Power Sources*, 2015, **282**, 194-201.
S24. W. Hu, R. Chen, W. Xie, L. Zou, N. Qin and D. Bao, *ACS applied materials & interfaces*, 2014, **6**, 19318-19326.
S25. F. Cai, R. Sun, Y. Kang, H. Chen, M. Chen and Q. Li, *RSC Advances*, 2015, **5**, 23073-23079.
S26. C.-S. Dai, P.-Y. Chien, J.-Y. Lin, S.-W. Chou, W.-K. Wu, P.-H. Li, K.-Y. Wu and T.-W. Lin, *ACS applied materials & interfaces*, 2013, **5**, 12168-12174.

S27. R. Rakhi, N. A. Alhebshi, D. Anjum and H. N. Alshareef, *Journal of Materials Chemistry A*, 2014, **2**, 16190-16198.
S28. L. Niu, Y. Wang, F. Ruan, C. Shen, S. Shan, M. Xu, Z. Sun, C. Li, X. Liu and Y. Gong, *Journal of Materials Chemistry A*, 2016, **4**, 5669-5677.
S29. R. Li, S. Wang, Z. Huang, F. Lu and T. He, *Journal of Power Sources*, 2016, **312**, 156-164.
S30. C. Xia, Q. Jiang, C. Zhao, P. M. Beaujuge and H. N. Alshareef, *Nano Energy*, 2016, **24**, 78-86.